frontiers | Frontiers in Membrane Science and Technology

TYPE Original Research
PUBLISHED 31 March 2023
DOI 10.3389/frmst.2023.1165678

OPEN ACCESS

EDITED BY
Anastasia Penkova,
Saint Petersburg State University, Russia

REVIEWED BY
Qusay Alsalhy,
University of Technology, Iraq
Stefan Chisca,
King Abdullah University of Science and Technology, Saudi Arabia

*CORRESPONDENCE
Heidi Richards,
nthunyalebea@gmail.com
Lebea N. Nthunya,
heidi.richards@wits.ac.za

SPECIALTY SECTION
This article was submitted to Membrane Applications—Liquid, a section of the journal Frontiers in Membrane Science and Technology

RECEIVED 14 February 2023
ACCEPTED 21 March 2023
PUBLISHED 31 March 2023

CITATION
Mpala TJ, Richards H, Etale A, Mahlangu OT and Nthunya LN (2023), Carbon nanotubes and silver nanoparticles modification of PVDF membranes for improved seawater desalination in direct contact membrane distillation.
Front. Membr. Sci. Technol. 2:1165678.
doi: 10.3389/frmst.2023.1165678

Carbon nanotubes and silver nanoparticles modification of PVDF membranes for improved seawater desalination in direct contact membrane distillation

Tshepiso J. Mpala[1], Heidi Richards[1]*, Anita Etale[2], Oranso T. Mahlangu[3] and Lebea N. Nthunya[1]*

[1]Molecular Sciences Institute, School of Chemistry, University of the Witwatersrand, Johannesburg, South Africa, [2]Department of Aerospace Engineering, School of Civil, Aerospace and Mechanical Engineering, University of Bristol, Bristol, South Africa, [3]Institute for Nanotechnology and Water Sustainability, College of Science, Engineering and Technology, University of South Africa, Johannesburg, South Africa

Membrane distillation (MD) has emerged as a novel technology capable of recovering fresh water from brackish, saline, and wastewater. However, its industrial application is limited to various challenges including membrane properties. In this work, the polyvinylidene fluoride (PVDF) membranes were modified to improve their performance towards desalination of simulated seawater particularly, acid treated carbon nanotubes (*f*-CNTs) and cellulose nanocrystals-capped silver nanoparticles (CNC-AgNPs) were incorporated into the PVDF matrix prior to casting. Simulated seawater (33.59 g/L) was used as the feed during DCMD tests. The modified membrane displayed improved tensile strength, surface roughness, and hydrophobicity. Interestingly, minimal leaching of AgNPs (0.378 ± 0.0628 ppm) was recorded within 72 h. Although water flux (0.179 ± 0.0303 kg/m^2/hr) remained relatively low, salt rejection (99.8%) improved upon incorporation of NPs. This provides a one-step solution towards better performance in MD for recovery of freshwater from high saline seawater.

KEYWORDS

desalination, carbon nanotubes, cellulose nanocrystals, membrane distillation, PVDF membranes, silver nanoparticles

1 Highlights

- PVDF membranes were prepared *via* phase separation process.
- To improve process performance, the membranes were modified with CNTs and CNC-capped AgNPs.
- Tensile strength, hydrophobicity and thermal stability of the PVDF membrane improved upon incorporation of NPs.
- Resulting membranes demonstrated improved performance in DCMD.

2 Introduction

Shortage of freshwater continues to threaten global socio-economic development despite abundant availability of saline water. However, desalination technologies are used to alleviate these challenges. Among others, reverse osmosis is the most utilized technology to recover freshwater from seawater. However, the high operational costs associated with this technology render it invalid for use in developing countries. For this reason, consideration of freshwater supply alternatives is imperative. MD emerged as a low-cost separation technology harnessed to treat high saline effluent for the recovery of potable water achieving separation efficiencies >99% (Hou et al., 2014). However, its industrial application is still limited to various factors, including production of low water fluxes and membrane fouling (Drioli, Ali and Macedonio, 2015). Although MD continues to be evaluated on laboratory scale for water desalination and treatment of wastewater, extensive studies are required to realize industrial operation (Lalia et al., 2014; Huang et al., 2021; Makanjuola, Anis and Hashaikeh, 2021; Rabie, Elkady and El-Shazly, 2021; Tian et al., 2021). Notably, pilot scale testing is actively underway in various research institutions (Tijing et al., 2015; Nthunya et al., 2022). Among others, Aquaver commissioned MD pilot plants in the Maldives (Drioli, Ali and Macedonio, 2015).

The mechanism of operation of MD includes the movement of vaporized water from the hot feed compartment to the cold distillate through a porous, hydrophobic membrane (Eryildiz et al., 2021). The membrane acts as a barrier, facilitating the separation of the feed water from the produced vapor (Tijing et al., 2015). The vapor pressure induced by the temperature difference across the two interface of the membrane acts as driving force (Eykens et al., 2017; Nthunya, Gutierrez, Derese, et al., 2019). Several hydrophobic membranes commonly used in MD include PVDF, polytetrafluoroethylene (PTFE) and polypropylene (PP) (Hou et al., 2014). Among these, PVDF possesses excellent hydrophobicity, thermal stability, mechanical strength and chemical resistance (Nthunya, Gutierrez, Verliefde, et al., 2019; Ji et al., 2021). In addition, PVDF dissolves in a myriad of organic solvents, dissimilar to PP and PTFE whose preparation require solvent choice and complex processing methods (Bottino, Capannelli and Comite, 2005).

For successful use in MD, PVDF membranes often require modification to improve process performance (Nejati et al., 2015; Mpala et al., 2022). Modification processes include incorporation of suitable nanoparticles to 1) improve membrane hydrophobicity and/or 2) fouling control measures. Leaper et al. (2018) modified PVDF with 3-(aminopropyl) triethoxysilane (APTS)- functionalized graphene oxide to improve the membranes' properties. Reportedly, an increase in surface and bulk membrane porosity was attained with an enhancement in mean pore-size. This translated to 86% increase in permeate flux. In another study, Kim et al. (2021) purified artificial seawater in vacuum membrane distillation (VMD) using polypropylene (PP)-modified PTFE. Notably, the membrane modification improved rate of water recovery and salt rejection (99.9%), achieving good agreement between computational and experimental results. Commonly used NPs including functionalized carbon nanotubes (*f*-CNTs) and silver nanoparticles (AgNPs) are incorporated into the various membranes not only to ensure resistance to thermal and mechanical stress but also to improve process performance. To ensure their safe use in water treatment, AgNPs require a facile environmentally benign preparation method (Nthunya et al., 2016; Nthunya, Gutrierrez and Mhlanga, 2022).

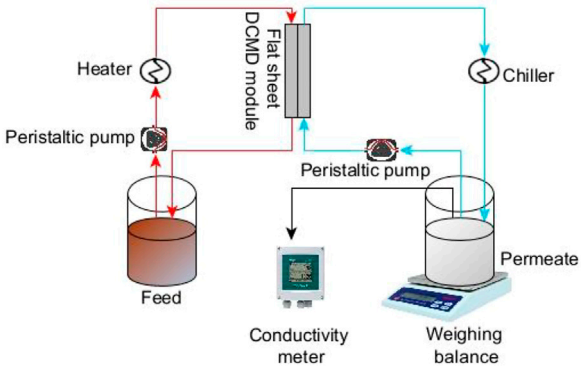

FIGURE 1
Experimental design for recovery of fresh water from salty water in direct contact membrane distillation.

In the current study, AgNPs were prepared from a CNC mediated method. Microwave irradiation process was carried out to improve homogenous dispersion of AgNPs on the capping CNCs. Dispersion of AgNPs on CNCs was reported elsewhere (Mpala et al., 2023). Cellulose nanocrystals (CNC's), commonly referred to as cellulose Nanowhiskers (CNW) or nanocrystalline celluloses (NCC's) are nano-structural forms of cellulose, the most abundant biopolymer in the environment (Naz, Ali and Zia, 2019; Amara et al., 2021). They exhibit enormous crystallinity (between 54% and 88%) with widths ranging from 4–70 nm, requiring acid hydrolysis (at high temperatures) for isolation (Brinchi et al., 2013; Naz, Ali and Zia, 2019). Moreover, CNCs are relatively elongated, rod shaped and less flexible (Brinchi et al., 2013). The CNCs can immobilize metal nanoparticles (MNPs), thus minimizing their leaching from supporting structures including PVDF membranes. To the best of our knowledge, AgNPs prepared *via* a greener microwave assisted irradiation with a simultaneous capping on CNCs ensuring minimal leaching from PVDF membranes is barely reported.

3 Materials and methods

3.1 Materials

PVDF (powder, Mw = 534,000 g/mol), polyvinylpyrrolidone (PVP, powder, Mw = 360,000 g/mol), dimethylformamide (DMF, ACS reagent, 99%), Dimethylacetamide (DMac, ACS reagent, 99%), 1-propanol (ACS reagent, 99%), sodium chloride (NaCl, Mw = 58.44 g/mol), magnesium chloride ($MgCl_2$, Mw = 95.21 g/mol), sodium sulphate ($NaSO_4$, Mw = 142.04 g/mol), calcium chloride ($CaCl_2$, Mw = 110.99 g/mol) and potassium chloride (KCl, Mw = 74.56 g/mol) were procured from Sigma Aldrich (Germany). The

TABLE 1 Casting solution composition for each membrane

Membrane	DMAc (g)	DMF (g)	PVDF (g)	PVP (g)	*f*-CNTs (g)	CNC-capped AgNP (g)
M1	51.0	34.0	15.0	-	-	-
M2	51.0	33.9	15.0	0.1	-	-
M3	50.6	33.8	15.0	0.1	0.5	-
M4	47.0	31.4	15.0	0.1	0.5	6

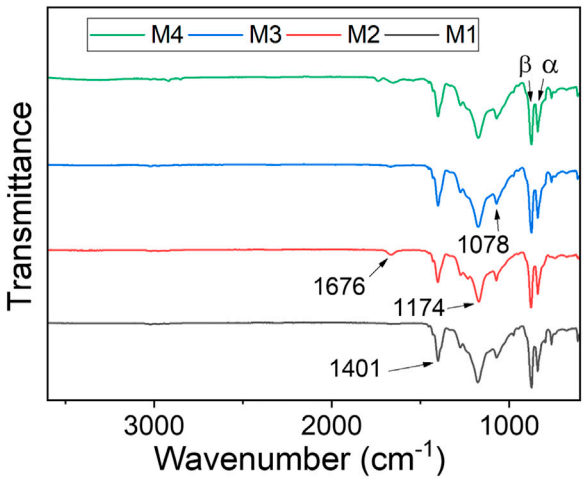

FIGURE 2
FTIR spectra of the as-synthesised membranes.

CNCs were procured from Nanografi Nano Technology and CNTs from SabiNano (Pty) Ltd.

3.2 Methods

3.3.1 Preparation of PVDF membranes

The PVDF membranes were prepared using phase inversion technique. Briefly, a solution of 15% PVDF was prepared using a mixed solvent system of DMAc/DMF (3:2 v/v ratio) and various non-solvent additives according to the requirements of each membrane (Table 1). The choice of mixed solvent system was based on reported literature. According to Karimi et al. (2020), diffusion rate of DMAc/DMF mixed solvent system is higher compared to DMSO and NMP, leading to formation of small pore sized membranes with finger-like structures. The polymer solution containing the reagents was stirred until full dissolution followed by degassing. Specifically, PVP and *f*-CNTs were blended with PVDF under magnetic stirring for 24 h (until attainment of homogenous solution). Afterwards, a solution of CNC-capped AgNPs was coated on the surface of the membrane during casting using a casting knife film applicator. The wet films were immersed in a water bath and coagulated for 24 h, followed by air-drying for 48 h.

3.3.2 Characterisation of PVDF membranes

The analyses of the as-synthesized membranes were carried out to understand their physicochemical properties. Dead-end filtration was used to determine the liquid entry pressure (LEP) of each membrane. Technically, 150 mL of de-ionized water was added into a membrane-equipped dead-end filtration cell. System pressure was gradually increased until the first water drop was recorded. This minimum pressure required to drive the water through the membrane was referred to as the LEP. Scanning electron microscopy (SEM) analysis was conducted using TESCAN Vega SEM at a voltage of 30 kV (kV) to understand the morphological properties of the membranes. Prior to SEM analysis, samples were sputter coated using gold/palladium (Au/Pd) to minimize sample charging. Atomic force microscopy (AFM, Witec Alpha 300 A, TS-150) was used at scanning area of 2.0 μm × 2.0 μm to evaluate membrane roughness. Fourier transform infrared spectroscopy (Tensor 27 FTIR, Bruker South Africa (PTY) LTD.) was used to evaluate the chemical composition of the membranes at a scanning range of 500 cm^{-1} to 4,000 cm^{-1}.

Membrane-water contact angle (WCA) was assessed using the sessile drop method. Approximately 5—8 μL of water was dropped on the membrane followed by contact angle measurement using a digital camera. Analysis was run in triplicates. Membrane porosity was determined gravimetrically using Equation (1). Also, the pore-size of the membranes was determined *via* filtration velocity method following Guerout-Elford-Ferry Equation (2):

$$\varepsilon = \frac{(m_1 - m_2)/D_e}{(m_1 - m_2)/D_e + m_2/D_p} \times 100, \quad (1)$$

Where ε is membrane porosity (%), m_1 and m_2 are the masses of the saturated membrane g) and dry membrane g) respectively, D_e and D_p are the specific gravities of 1-propanol (g/cm^3) and PVDF (g/cm^3), respectively.

$$r_m = \frac{\sqrt{(2.9 - 1.75\varepsilon)8\mu\delta Q}}{\varepsilon.A.\Delta P} \times 100, \quad (2)$$

Where rm is the mean pore radius m), ε is the porosity, μ is the viscosity of water (0.001 Pas), δ is the membrane thickness m), Q is the volume of filtrate per unit time (m3/s), A is the membrane area (m2) and Δ P is the pressure (Pa).

3.3.3 Leaching studies of AgNPs

A modified method was used to quantify amount of AgNPs released from CNC/AgNP-modified PVDF membrane (M4) (Xuan et al., 2020). Briefly, prepared membrane was cut into rectangles (1 × 3 cm), placed in 15 mL DI water, and shaken at 140 rpm for 72 h. Aliquot samples of 3 mL were taken at different time intervals (1, 3, 6, 9, 12, 24, 48 and 72 h), with an equal supplement of fresh DI water. The collected aliquots were analyzed for silver using inductively coupled plasma optical emission spectroscopy (ICP-OES).

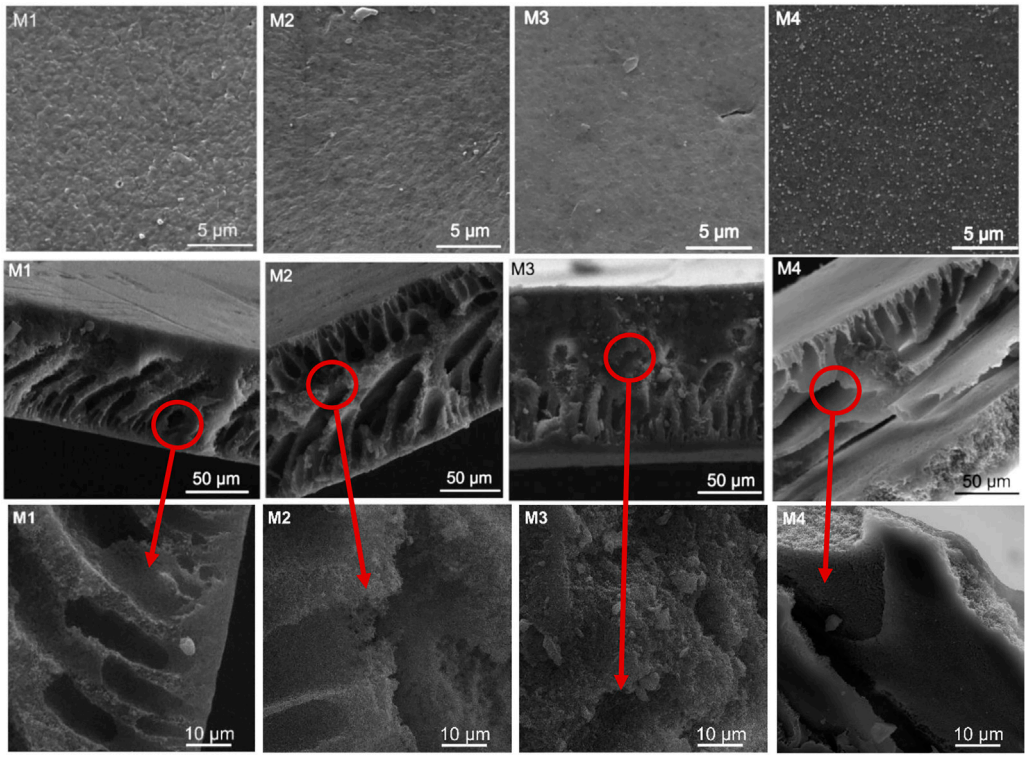

FIGURE 3
SEM micrographs of PVDF membranes: Top surface and corresponding cross-sectional morphology.

TABLE 2 Physical properties of the as-synthesised membranes

	Overall porosity (%)	LEP (kPa)	Overall Thickness (μm)	Mean pore size (μm)
M1	72.6 ± 0.84	310 ± 7	86	0.17
M2	84.3 ± 1.15	280 ± 3	112	0.21
M3	71.1 ± 2.99	340 ± 6	124	0.10
M4	70.4 ± 1.09	330 ± 1	135	0.10

3.3.4 Evaluation of MD process performance using synthetic membranes

Lab-scale DCMD tests were conducted to evaluate membrane performance (Figure 1). The active surface area for each membrane tested was 1.147 m^2. Artificial seawater (the feed stream) was composed of 24.5 g/L NaCl, 5.2 g/L MgCl2, 4.1 g/L NaSO4, 1.1 g/L CaCl2, and 0.69 g/L KCl. Distilled water (approx. conductivity of 0.691 μS/cm) was used as the permeate stream. The plate and frame membrane module was used during operation. The solutions were circulated in a counter-current direction at a crossflow velocity of 7 mL/s using a peristaltic pump (Cole Parmer Ltd., Masterflex). The feed and permeate solution temperatures were set at 60°C and 15°C, respectively. Salt rejection (R%) and permeate flux (J) were calculated using Equations (3), (4) respectively.

$$R\% = \frac{k_f - k_p}{k_f} * 100\%, \tag{3}$$

$$J = \frac{m}{A*t}, \tag{4}$$

where $R\%$, k_f, k_p J, m, A, t represents the salt rejection (%), feed conductivity (μS/cm), permeate conductivity (μS/cm), water flux (kg/m^2·h), permeate mass obtained from the digital balance (kg), effective membrane area (m^2) and time (h) respectively. Each of these parameters were obtained as per schematic illustration presented in Figure 1.

4 Results and discussion

4.1 Chemical composition of PVDF membranes

FTIR analysis of the as-synthesized membranes was carried out to understand their chemical composition. The individual membranes exhibited similar peaks with minimal differences

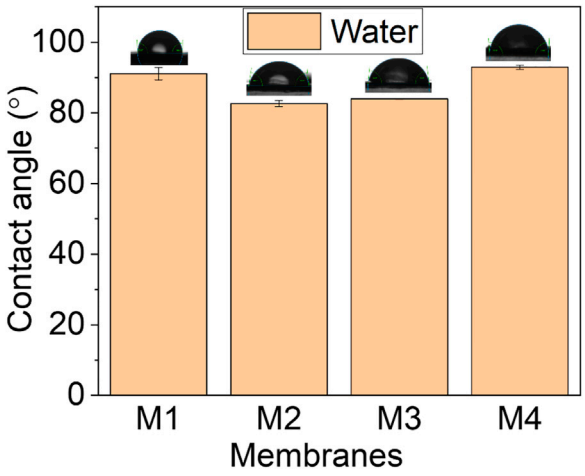

FIGURE 4
Contact angle measurements of the membranes.

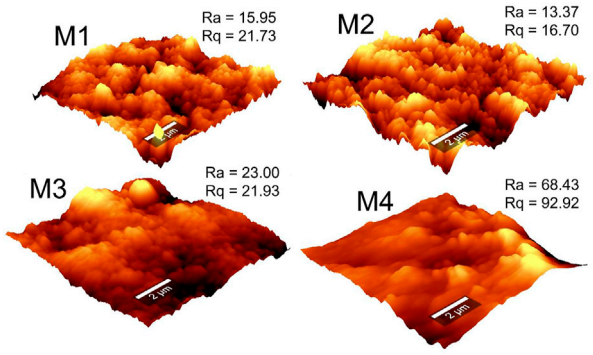

FIGURE 5
Surface roughness characteristics of PVDF membranes.

(Figure 2) where, 1,078 cm^{-1}, 1,174 cm^{-1}, 1,401 cm^{-1} were assigned to C-C stretching, intense C-F stretching, and C-H wagging and stretching vibration respectively (Tan et al., 2020; Lu et al., 2021). Indeed, the fingerprint region of PVDF was reported at 600—1,500 cm^{-1} (Teoh et al., 2021). The weak stretch at 1,676 cm^{-1} caused by the presence of C=O for M2, M3 and M4 confirmed the presence of PVP within the modified PVDF membrane. The CNC/AgNP-modified PVDF membrane displayed the α and β phases of PVDF at 838 cm^{-1} and 871 cm^{-1}, respectively, with the β phase existing in the highest intensity. This was attributed to AgNPs' interaction with PVDF (Issa et al., 2017).

4.2 Morphological properties of PVDF membranes

The SEM micrographs of the PVDF membranes illustrating their morphological properties are presented in Figure 3. The top surfaces of all membranes appeared sponge-like, with highly compact surfaces. The sponge-like structure present mechanical strength of the membrane (Lai et al., 2014). No evidence of membrane deformation was detected. Incorporation of CNC-capped AgNPs on PVDF resulted in minimal particle agglomeration (Figure 3, M4). This is undesirable as agglomeration reduces the activity of nanoparticles (NPs), further minimizing membrane performance. Since all membrane surfaces appeared dense, structural variations were assessed using cross-sectional morphology images and AFM.

Based on the cross-sectional images, the membranes were asymmetric and exhibited heterogenous structures containing distinct macro-voids of different shapes and sizes (Figure 3). This was attributed to the difference in solution compositions of the synthesised membranes (Table 1). Although the addition of PVP induced the formation of finger-like macropores (M2) due to its hydrophilicity, addition of *f*-CNTs lowered the size and number of these structures (M3). This was associated to an increase in the viscosity of the polymer solution and a subsequent decrease in the solvent/non-solvent exchange rate during phase inversion (Nejati et al., 2015). Water was used as the coagulating agent during synthesis because of its ability to rapidly facilitate the solvent/non-solvent exchange rate (Teoh et al., 2021). Further addition of CNC-capped AgNPs increased pore elongation, especially for the top layer of the membrane. This was attributed to the hydrophilicity of the NPs (Xu et al., 2020). Generally, asymmetric structures of membranes translate to enhanced permeability (Wu et al., 2015). The AgNPs were uniformly dispersed on the surface of the membrane as per top surface micrograph of M4. This was a result of AgNPs capping and uniform distribution on the CNCs as per TEM micrographs presented elsewhere (Mpala et al., 2023). Interestingly, there was no structural deformation for all synthesised membranes.

4.3 Physical properties of PVDF membranes

Incorporation of the *f*-CNTs and CNC-capped AgNPs improved the membranes' resistance towards passage of liquid water (Table 2). This is evident from the increased LEP. Specifically, the LEP of M1, M2, M3, and M4 were 310 ± 7 kPa 280 kPa ± 3, 340 kPa ± 6, and 330 kPa ± 1, respectively. According to Chiu et al. (2021), addition of *f*-CNTs increases viscosity of PVDF polymer solution, thus leading to a decreased exchange rate of the solvent (DMac/DMF 3:2) and non-solvent (water) during phase inversion (Chiu et al., 2021). Decreased solvent exchange rate reduced overall membrane porosity and pore size (Table 2). Polymer solution demixing rate depends on various parameters including polymer affinity to the solvent and the solution concentration. As per ternary diagrams, reduced affinity of polymer to the solvent increases demixing rate (Alibakhshi et al., 2019). The decrease in LEP and contact angle from M1 to M2 was attributed to the addition of PVP, largely due to its high polarity and water solubility (Rawat et al., 2014), causing a rise in the thermodynamic instability of the polymer solution during casting (Eren and Güney, 2019). Consequently, an instantaneous demixing of the solvent and non-solvent occurred, leading to the formation of large macropores (Figure 3). This was simultaneously proven by an increased membrane pore size (M2—0.21 µm) (Tofighy, Mohammadi and Sadeghi, 2021). Notably, an increase

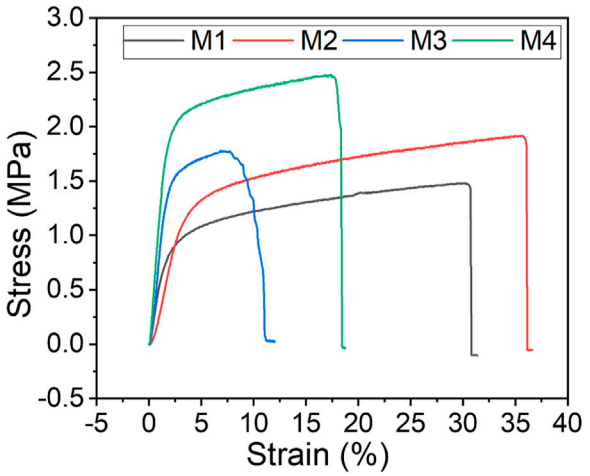

FIGURE 6
Stress-strain plot of the as-synthesised membranes.

in overall porosity and reduction in membrane pore sizes were inversely proportional to LEP, a relation directly confirmed by Ardeshiri et al. (2018). Nanofillers such as *f*-CNTs reduce the membranes pores and porosity by filling the micro-voids, thus causing an increase in LEP (Zhou et al., 2019). Also, the LEP depends on pore microstructure and length. Specifically, membranes characterized by high tortuosity give rise to high LEP (Wu et al., 2018). This was evident as LEP increased with an increase in membrane thickness. High LEP of membranes ensures resistance to wetting by process liquids, thus promoting high salt rejection in water desalination.

4.4 Membrane-water contact angle (WCA)

Membrane hydrophobicity was determined using WCA measurements, where the interaction of water with the membrane surface was measured (Figure 4). The WCA of pristine PVDF membrane was 91.1° ± 0.80. Similar results were reported by Isya et al. (2020). Due to PVDF's fluorinated carbons, the membrane possesses WCA ˃90 ℃. However, to improve their performances in MD, PVDF membranes require modification (Sinha Ray, Dangayach and Kwon, 2021). To increase membrane pore sizes, water soluble PVP was used to modify PVDF membranes. The WCA decreased from 91.1 ± 0.80° to 82.6 ± 0.95°. Upon the addition of NPs (i.e., *f*-CNTs and CNC-AgNPs), the WCA increased to 92.9 ± 0.35°, implying enhanced hydrophobicity. This was attributed to the hydrophobic nature of the *f*-CNTs and the increased surface roughness as confirmed by AFM results (Figure 5). Rough membrane surfaces possess air-pockets lowering the surface energy and minimizing interaction with polar solvents (Teoh et al., 2021). The direct correlation between hydrophobicity and surface roughness was noted elsewhere (Zheng et al., 2016).

4.5 Surface roughness of PVDF membranes

The AFM micrographs were used to evaluate membrane surface roughness (Figure 5). The micrographs displayed bright regions (signifying peaks) and dark regions (signifying valleys). According to the Cassie Baxter phenomenon, valleys act as air-pockets that reduce the surface energy and interfacial tension, thus increasing membrane-water contact angles (Teoh et al., 2021). The surface roughness (Ra) and root mean square roughness (Rq) were used to estimate membrane-liquid interactions. Upon addition of PVP in the casting solution, the average surface roughness decreased from 15.95 nm (M1) to 13.37 nm (M2) due to formation of a smooth surface. However, a considerable increase in surface roughness was recorded (68.43 nm) upon addition of *f*-CNTs and CNC-capped AgNPs (i.e., M4). This increase was attributed to adherence of the NPs to the network of the polymer. These changes in membrane roughness cohere with WCA measurements. In MD, rough membranes necessitate increased turbulence of the feed solution, thus lowering the heat transfer resistance at the boundary layer and facilitating better vapor transport (Pagliero et al., 2021).

4.6 Mechanical properties of PVDF membranes

Evaluation of membrane mechanical properties to determine their suitability in MD systems is key as membrane durability affects costs of operation (Lalia et al., 2014). Herein, tensile strength (MPa), elongation stretch (%), and yield strength (MPa) were used to assess the mechanical properties of the as-synthesised membranes (Figure 6; Table 3). Based on the stress-strain plot, the mechanical strength of M1 (pristine PVDF) increased by 75% upon addition of PVP, *f*-CNTs and CNC-capped AgNPs from 0.4637 MPa to 1.0811 MPa. This was due to the excellent dispersity of NPs within the PVDF matrix and the NPs higher affinity for PVDF (Nassrullah et al., 2020; Tabhane and Giripunje, 2020). Excellent dispersity transfers the load from PVDF to the NPs, thus increasing mechanical strength of the membranes (Dlamini, Mamba and Li, 2019). Owing to their high mechanical strength, CNCs were eminent in increasing the tensile strength of the PVDF

TABLE 3 Mechanical properties of the membranes

Membranes	Ultimate tensile strength (MPa)	Young's modulus (MPa)	Elongation stretch (%)	Yield strength (MPa)
M1	1.477	0.2694	15.56	0.9576
M2	1.9121	0.4637	15.65	1.422
M3	1.7747	0.4606	5.95	1.578
M4	2.4740	1.0811	9.31	2.075

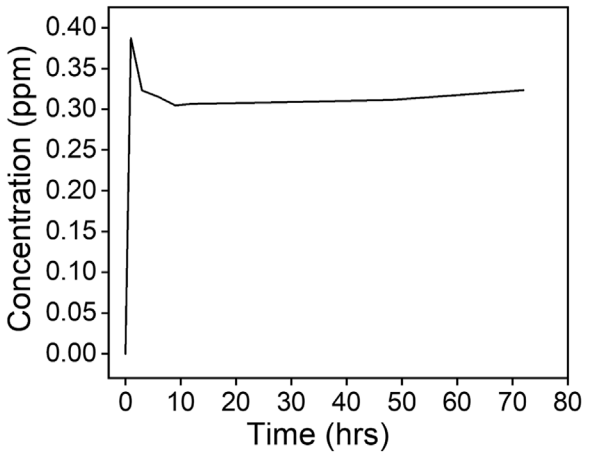

FIGURE 7
Concentration of silver of CNC/AgNP-modified PVDF membrane (M4) following a 72-h silver leaching test.

membranes (Grishkewich et al., 2017; Mbakop, Nthunya and Onyango, 2021). Also, addition of the pore forming PVP increased the membrane tensile strength to 0.4637 MPa due to formation of stress terminating pores.

4.7 The AgNPs leaching assessment

To assess the stability of capped AgNPs, leaching tests were evaluated using DI water. Although high activities are reported upon release of AgNPs from the capping materials, uncontrolled release may: 1) reduce the effectiveness of the membrane within a short time, 2) contaminate the distillate, and 3) cause regular membrane replacement due to activity deterioration, thus increasing operational expenditure (Barrios et al., 2020). Due to its toxicity, leachability studies of AgNPs are required to assess their environmental implications. The leaching of AgNPs from M4 was evaluated at various intervals for 72 h (Figure 7). Approximately, 0.378 ± 0.0628 ppm was released from the membrane, with gradual decline as a function of time. This suggests long term stability of the NPs (Xuan et al., 2020). The release of high concentrations at initial stages of operation was caused by weakly bound or excess AgNPs (Qi et al., 2021). These results ascertain the applicability of the modified membrane for long term application in MD. Similarly, minimal release of AgNPs was reported by Maharubin et al. (2018), noting a 0.918 ppm concentration in the permeate.

4.7.1 Evaluation of membrane performance in direct contact membrane distillation (DCMD)

The performance of the membranes (M1, M2, M3, M4) was evaluated in a DCMD lab-scale set-up where artificial seawater was used as the feed solution. Water flux and permeate conductivity profiles are presented in Figure 8. The water flux (0.528 ± 0.0838 kg/m^2/hr) of the pristine membrane (M1) remained stable for 24 h. However, permeate conductivity increased gradually without exceeding 85 µS/cm. This demonstrated excellent salt rejection efficiency, averaging to 99.8%. The M2 presented the highest flux in comparison to the other membranes (0.603 ± 0.157 kg/m^2/hr), specifically due to high membrane porosity and low LEP (Table 2) caused

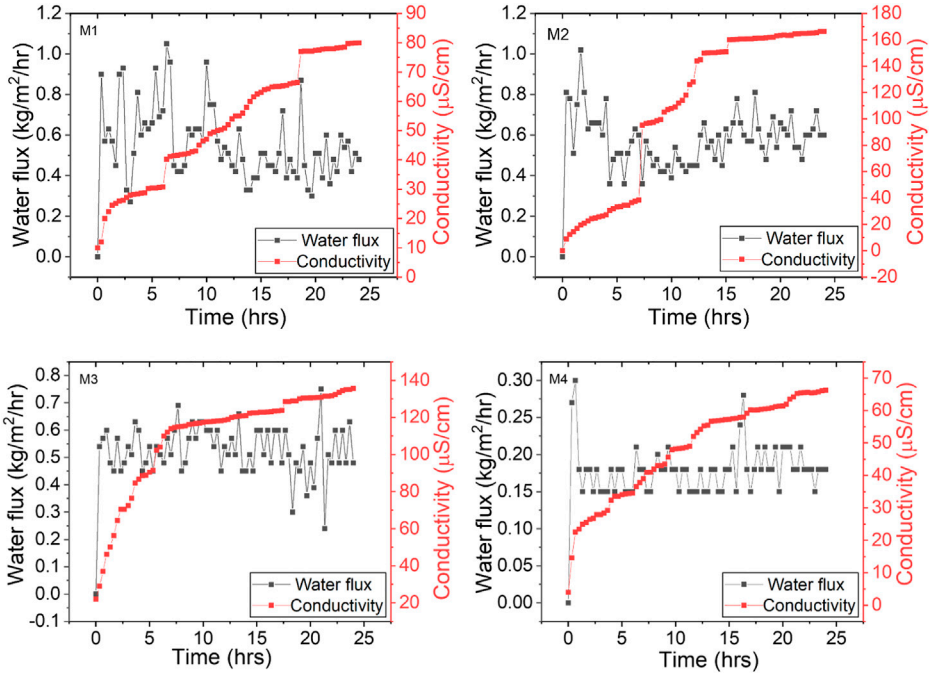

FIGURE 8
Conductivity and water flux for M1, M2, M3 and M4 using synthetic seawater in DCMD.

TABLE 4 Comparison of recent studies assessing MD performance using artificial seawater

MD configuration	Membrane material	Feed Stream – Artificial seawater concentration:	Operating conditions: Feed temperature (FT), Permeate temperature (PT) and flowrate (FL)	Water flux (WF - kg/m^2 × hr) and salt rejection efficiency (SRE)	Reference
VMD	PTFE-PP composite	60 g/kg	FT – 60 °C	WF – 17.5	(Kim et al., 2021)
			PT –	SRE – 99.9%	
			FL – 0.7 L/min		
DCMD	PVDF	35.0 g/L	FT – 65 °C	WF – 9.90	Mustafa *et al.* (2021)
			PT – 25 °C	SRE – 99.0%	
			FL – 0.10 L/min		
SGMD	PVDF	29.2 g/L	FT – 25 °C	WF – 0.64	Avci *et al.* (2021)
			PT –	SRE –	
			FL – 20 L/min		
DCMD	PVDF	35.1 g/L	FT – 70 °C	WF – 40.3	Kim *et al.* (2020)
			PT – 20 °C	SRE –	
			FL – 0.5 L/min		
VMD	PVDF	35.0 g/L	FT – 25 °C	WF – 2.5	(Zhou et al., 2019)
			PT –	SRE – 99.9%	
			FL –		
AGMD	PVDF	35.0 g/L	FT – 85 °C	WF – 3.4	(Leaper et al., 2018)
			PT – 20 °C	SRE – 99.7%	
			FL – 0.38 L/min		
VMD	PP	40.0 g/L	FT – 50 °C	WF – 9.95	Kim, Thu and Choi (2015)
			PT –	SRE –	
			FL – 0.6 m/s		
DCMD	PVDF	33.5 g/L	FT – 60 °C	WF – 0.52	This work
			PT – 15 °C	SRE – 99.8%	
			FL – 0.41 L/min		

by the presence of PVP. Similarly, conductivity increased significantly to 166.2 μS/cm, registering poor salt rejection. The high conductivity implied occurrence of membrane wetting leading to the passage of dissolved salts through the membrane pores. According to Teoh et al. (2021), an increase in distillate conductivity above 20 μS/cm demonstrates the initial wetting of the membrane. Ahn et al. (2021) reported similar results, where PVDF membranes presented low salt rejection with high water flux in DCMD. Although the distillate conductivity for M2 was high, excellent salt rejection (99.6%) was recorded, largely due to the hydrophobic nature of the PVDF membrane.

While M4 was characterized by high WCA and LEP, the average water flux obtained was the lowest (0.179 ± 0.0303 kg/m^2/hr). This was attributed to the blockage of pores induced by the presence of the NPs on the surface and inner pores of the membrane. The decrease in pore sizes induced a mass transfer resistance (Huang et al., 2021). However, the salt rejection of M4 was excellent (99.8%), with the conductivity increasing to 68.2 μS/cm within the 24 h operation period. This was attributed to the hydrophobic nature of the membrane, ensuring passage of vaporized water (Figure 4). Hydrophobicity provides resistance of liquid water transfer due to low surface tension, decreasing the surface energy and subsequently increasing its water-repellence (Zheng et al., 2016). As a result, the

mass transfer is facilitated by vapour formation. The failure to attain 99.999% was due to formation hydration layer on M4 caused by presence of hydrophilic CNC-capped AgNPs. Therefore, various modification methods should be explored to ensure maximized process performance. Nonetheless, the findings of this study are comparable to the existing literature where excellent salt rejection is attained (Table 4).

5 Conclusion

Water scarcity has motivated the quest for the development of new and sustainable water purification systems. MD is an emerging membrane separation technology harnessed to recover fresh water from contaminated wastewaters. Although MD possesses attractive features, its industrial application is limited to various factors, affecting process performance. In this work, PVDF was synthesized using the phase inversion technique and functionalized with *f*-CNTs and CNC-AgNPs to improve membrane properties. Incorporation of the NPs improved membrane hydrophobicity, tensile strength, and surface roughness. Specifically, WCA of the membranes increase from 91.1° (M1) to 92.9° (M4), indicating slight increase in hydrophobicity. Also, LEP of the membranes increased from 310 kPa to 330 kPa due to the decrease in membrane pore size and increase in hydrophobicity. Technically, the MD process should be operated at circulation pressure below LEP of the membrane. Hydrophobic membranes with high LEP improves membrane resistance to wetting, thus ensuring high salt rejection. Minimal leaching of AgNPs was reported (380 ppb), indicating satisfactory capping and support on the membrane surface. Although membrane properties were improved, the water flux remained low. This was attributed to high mass resistance induced by small pore formation because of NPs incorporation. However, salt rejection remained relatively high, markedly at 99.8%. Therefore, *f*-CNTs and CNC-AgNPs modification of PVDF with will open research directions toward application in membrane-based technologies.

Data availability statement

The original contributions presented in the study are included in the article/Supplementary Material, further inquiries can be directed to the corresponding authors.

Author contributions

LN, AE, and HR contributed to conception and design of the study. LN and HR organized the database. OM performed membrane characterization and statistical analysis. TM wrote the first draft of the manuscript. TM and LN wrote sections of the manuscript. All authors contributed to manuscript revision, read, and approved the submitted version.

Funding

The authors would like to thank the University of the Witwatersrand and National Research Foundation (NRF-grant number: 132724) for funding this research work.

Conflict of interest

The authors declare that the research was conducted in the absence of any commercial or financial relationships that could be construed as a potential conflict of interest.

Publisher's note

All claims expressed in this article are solely those of the authors and do not necessarily represent those of their affiliated organizations, or those of the publisher, the editors and the reviewers. Any product that may be evaluated in this article, or claim that may be made by its manufacturer, is not guaranteed or endorsed by the publisher.

References

Ahn, M., Cho, H., Choi, Y., Lee, S., and Lee, S. (2021). Analysis of polyvinylidene fluoride membranes fabricated for membrane distillation. *Membranes* 11 (6), 437. doi:10.3390/membranes11060437

Alibakhshi, S., Youssefi, M., Hosseini, S. S., and Zadhoush, A. (2019). Tuning morphology and transport in ultrafiltration membranes derived from polyethersulfone through exploration of dope formulation and characteristics. *Mater. Res. Express* 6 (12), 125326–125414. doi:10.1088/2053-1591/ab56c3

Amara, C., El Mahdi, A., Medimagh, R., and Khwaldia, K. (2021). Nanocellulose-based composites for packaging applications. *Curr. Opin. Green Sustain. Chem.* 31, 100512. doi:10.1016/j.cogsc.2021.100512

Ardeshiri, F., Salehi, S., Peyravi, M., Jahanshahi, M., Amiri, A., and Rad, A. S. (2018). PVDF membrane assisted by modified hydrophobic ZnO nanoparticle for membrane distillation. *Asia-Pacific J. Chem. Eng.* 13 (3), 21966–e2212. doi:10.1002/apj.2196

Avci, A. H., Santoro, S., Politano, A., Propato, M., Micieli, M., Aquino, M., et al. (2021). Photothermal sweeping gas membrane distillation and reverse electrodialysis for light-to-heat-to-power conversion. *Chem. Eng. Process. - Process Intensif.* 164 (January), 108382. doi:10.1016/j.cep.2021.108382

Barrios, A. C., Carrillo, D., Waag, T. R., Rice, D., Bi, Y., Islam, R., et al. (2020). Prolonging the antibacterial activity of nanosilver-coated membranes through partial sulfidation. *Environ. Sci. Nano* 7 (9), 2607–2617. doi:10.1039/d0en00300j

Bottino, A., Capannelli, G., and Comite, A. (2005). Novel porous poly (vinylidene fluoride) membranes for membrane distillation. *Desalination* 183 (1–3), 375–382. doi:10.1016/j.desal.2005.03.040

Brinchi, L., Cotana, F., Fortunati, E., and Kenny, J. M. (2013). Production of nanocrystalline cellulose from lignocellulosic biomass: Technology and applications. *Carbohydr. Polym.* 94 (1), 154–169. doi:10.1016/j.carbpol.2013.01.033

Chiu, F. C., Behera, K., Cai, H. J., and Chang, Y. H. (2021). Polycarbonate/poly(Vinylidene fluoride)-blend-based nanocomposites—Effect of adding different carbon nanofillers/organoclay. *Polymers* 13 (16), 2626–2715. doi:10.3390/polym13162626

Dlamini, D. S., Mamba, B. B., and Li, J. (2019). The role of nanoparticles in the performance of nano-enabled composite membranes – a critical scientific perspective. *Sci. Total Environ.* 656, 723–731. doi:10.1016/j.scitotenv.2018.11.421

Drioli, E., Ali, A., and Macedonio, F. (2015). Membrane distillation: Recent developments and perspectives. *Desalination* 356, 56–84. doi:10.1016/j.desal.2014.10.028

Eren, B., and Güney, M. (2019). The role of polyvinylpyrrolidone as a pore former on microstructure and performance of polysulfone membranes. *Bilecik*

Şeyh Edebali Üniversitesi Fen Bilim. Derg. 6 (September). doi:10.35193/bseufbd.589808

Eryildiz, B., Ozbey-Unal, B., Gezmis-Yavuz, E., Koseoglu-Imer, D. Y., Keskinler, B., and Koyuncu, I. (2021). Flux-enhanced reduced graphene oxide (rGO)/PVDF nanofibrous membrane distillation membranes for the removal of boron from geothermal water. *Sep. Purif. Technol.* 274, 119058–8. doi:10.1016/j.seppur.2021.119058

Eykens, L., De Sitter, K., Dotremont, C., Pinoy, L., and Van der Bruggen, B. (2017). Membrane synthesis for membrane distillation: A review. *Sep. Purif. Technol.* 182, 36–51. doi:10.1016/j.seppur.2017.03.035

Grishkewich, N., Mohammed, N., Tang, J., and Tam, K. C. (2017). Recent advances in the application of cellulose nanocrystals. *Curr. Opin. Colloid Interface Sci.* 29, 32–45. doi:10.1016/j.cocis.2017.01.005

Hou, D., Fan, H., Jiang, Q., Wang, J., and Zhang, X. (2014). Preparation and characterization of PVDF flat-sheet membranes for direct contact membrane distillation. *Sep. Purif. Technol.* 135, 211–222. doi:10.1016/j.seppur.2014.08.023

Huang, Y. X., Liang, D. Q., Luo, C. H., Zhang, Y., and Meng, F. (2021). Liquid-like surface modification for effective anti-scaling membrane distillation with uncompromised flux. *J. Membr. Sci.* 637 (July), 119673. doi:10.1016/j.memsci.2021.119673

Issa, A., Al-Maadeed, M., Luyt, A., Ponnamma, D., and Hassan, M. (2017). Physico-mechanical, dielectric, and piezoelectric properties of PVDF electrospun mats containing silver nanoparticles. *C* 3 (4), 30. doi:10.3390/c3040030

Ji, J., Mazinani, S., Ahmed, E., John Chew, Y., and Mattia, D. (2021). Hydrophobic poly(vinylidene fluoride)/siloxene nanofiltration membranes. *J. Membr. Sci.* 635 (February), 119447. doi:10.1016/j.memsci.2021.119447

Karimi, A., Khataee, A., Vatanpour, V., and Safarpour, M. (2020). The effect of different solvents on the morphology and performance of the ZIF-8 modified PVDF ultrafiltration membranes. *Sep. Purif. Technol.* 253 (April), 117548. doi:10.1016/j.seppur.2020.117548

Kim, H., Yun, T., Hong, S., Lee, S., Jeong, S., et al. (2020). Retardation of wetting for membrane distillation by adjusting major components of seawater. *Water Res.* 175, 115677. doi:10.1016/j.watres.2020.115677

Kim, H., Yun, T., Hong, S., and Lee, S. (2021). Experimental and theoretical investigation of a high performance PTFE membrane for vacuum-membrane distillation. *J. Membr. Sci.* 617, 118524. doi:10.1016/j.memsci.2020.118524

Kim, Y. D., Thu, K., and Choi, S. H. (2015). Solar-assisted multi-stage vacuum membrane distillation system with heat recovery unit. *Desalination* 367, 161–171. doi:10.1016/j.desal.2015.04.003

Lai, C. Y., Groth, A., Gray, S., and Duke, M. (2014). Preparation and characterization of poly(vinylidene fluoride)/nanoclay nanocomposite flat sheet membranes for abrasion resistance. *Water Res.* 57, 56–66. doi:10.1016/j.watres.2014.03.005

Lalia, B. S., Guillen, E., Arafat, H. A., and Hashaikeh, R. (2014). Nanocrystalline cellulose reinforced PVDF-HFP membranes for membrane distillation application. *Desalination* 332, 134–141. doi:10.1016/j.desal.2013.10.030

Leaper, S., Abdel-Karim, A., Faki, B., Luque-Alled, J. M., Alberto, M., Vijayaraghavan, A., et al. (2018). Flux-enhanced PVDF mixed matrix membranes incorporating APTS-functionalized graphene oxide for membrane distillation. *J. Membr. Sci.* 554 (March), 309–323. doi:10.1016/j.memsci.2018.03.013

Lu, Y., Ma, Y., Yang, T., and Guo, J. (2021). Hydrophilic modification of PVDF membranes by *in situ* synthesis of nano-Ag with nano-ZrO2. *Green Process. Synthesis* 10 (1), 538–546. doi:10.1515/gps-2021-0050

Maharubin, S., Zhou, Y., and Tan, G. Z. (2018). Development and investigation on a silver nanoparticle-incorporated electrofiltration system for biofouling control. *IEEE Trans. Nanotechnol.* 17 (5), 948–954. doi:10.1109/TNANO.2018.2832210

Makanjuola, O., Anis, S. F., and Hashaikeh, R. (2021). Enhancing DCMD vapor flux of PVDF-HFP membrane with hydrophilic silica fibers. *Sep. Purif. Technol.* 263, 118361. doi:10.1016/j.seppur.2021.118361

Mbakop, S., Nthunya, L. N., and Onyango, M. S. (2021). Recent advances in the synthesis of nanocellulose functionalized-hybrid membranes and application in water quality improvement. *Processes* 9 (4), 611–624. doi:10.3390/pr9040611

Mpala, T. J., Etale, A., Richards, H., and Nthunya, L. N. (2022). Biofouling phenomena in membrane distillation: Mechanisms and mitigation strategies. *Environ. Sci. Adv.* 2, 39–54. doi:10.1039/d2va00161f

Mpala, T. J., Serepa-Dlamini, M. H., Etale, A., Richards, H., and Nthunya, L. N. (2023). Cellulose nanocrystal-mediated synthesis of silver nanoparticles via microwave assisted method for biofouling control in membrane distillation. *Mater. Today Commun.* 34, 105028. doi:10.1016/j.mtcomm.2022.105028

Mustafa, I., Kilibay, A., Alhseinat, E., and Almarzooqi, F. (2021). Enhanced membrane distillation water flux through electromagnetism. *Chem. Eng. Process. - Process Intensif.* 169 (March), 108597. doi:10.1016/j.cep.2021.108597

Nassrullah, H., Makanjuola, O., Janajreh, I., AlMarzooqi, F. A., and Hashaikeh, R. (2020). Incorporation of nanosized LTL zeolites in dual-layered PVDF-HFP/cellulose membrane for enhanced membrane distillation performance. *J. Membr. Sci.* 611 (April), 118298. doi:10.1016/j.memsci.2020.118298

Naz, S., Ali, J. S., and Zia, M. (2019). Nanocellulose isolation characterization and applications: A journey from non-remedial to biomedical claims. *Bio-Design Manuf.* 2 (3), 187–212. doi:10.1007/s42242-019-00049-4

Nejati, S., Boo, C., Osuji, C. O., and Elimelech, M. (2015). Engineering flat sheet microporous PVDF films for membrane distillation. *J. Membr. Sci.* 492, 355–363. doi:10.1016/j.memsci.2015.05.033

Nofitri Da Conceicao Isya, H., Valadares Marcal, I., and Aquino, R. R. (2020). Fabrication and characterization of PVDF with an additive of nanozeolite via electrospinning and non-solvent induced phase separation (NIPS) process. *MATEC Web Conf.* 319, 10002. doi:10.1051/matecconf/202031910002

Nthunya, L. N., Bopape, M. F., Mahlangu, O. T., Mamba, B. B., Van der Bruggen, B., Quist-Jensen, C. A., et al. (2022). Fouling, performance and cost analysis of membrane-based water desalination technologies: A critical review. *J. Environ. Manag.* 301, 113922. doi:10.1016/j.jenvman.2021.113922

Nthunya, L. N., Gutierrez, L., Derese, S., Nxumalo, E. N., Verliefde, A. R., Mamba, B. B., et al. (2019). A review of nanoparticle-enhanced membrane distillation membranes: Membrane synthesis and applications in water treatment. *Chem. Technol. Biotechnol.* 94 (9), 2757–2771. doi:10.1002/jctb.5977

Nthunya, L. N., Gutierrez, L., Verliefde, R., and Mhlanga, S. D. (2019). Enhanced flux in direct contact membrane distillation using superhydrophobic PVDF nanofibre membranes embedded with organically modified SiO2 nanoparticles. *Chem. Technol. Biotechnol.* 94 (9), 2826–2837. doi:10.1002/jctb.6104

Nthunya, L. N., Gutrierrez, L., and Mhlanga, S. D. (2022). "Bio-mediated synthesis of silver nanoparticles via conventional and irradiation-assisted methods and their application for environmental remediation in agriculture," in *Green synthesis of silver nanomaterials* (Netherlands: Elsevier B.V), 1–21. doi:10.1016/B978-0-12-824508-8.00020-4

Nthunya, L. N., Masheane, M. L., Malinga, S. P., Barnard, T. G., Nxumalo, E. N., Mamba, B. B., et al. (2016). UV-assisted reduction of *in situ* electrospun antibacterial chitosan-based nanofibres for removal of bacteria from water. *RSC Adv.* 6, 95936–95943. doi:10.1039/C6RA19472A

Pagliero, M., Comite, A., Soda, O., and Costa, C. (2021). Effect of support on PVDF membranes for distillation process. *J. Membr. Sci.* 635 (January), 119528. doi:10.1016/j.memsci.2021.119528

Qi, L., Jiang, T., Liang, R., and Qin, W. (2021). Polymeric membrane ion-selective electrodes with anti-biofouling properties by surface modification of silver nanoparticles. *Sensors Actuators, B Chem.* 328 (October), 129014. doi:10.1016/j.snb.2020.1290142020

Rabie, M., Elkady, M. F., and El-Shazly, A. H. (2021). Effect of channel height on the overall performance of direct contact membrane distillation. *Appl. Therm. Eng.* 196 (February), 117262. doi:10.1016/j.applthermaleng.2021.117262

Rawat, A., Mahavar, H. K., Tanwar, A., and Singh, P. J. (2014). Study of electrical properties of polyvinylpyrrolidone/polyacrylamide blend thin films. *Bull. Mater. Sci.* 37 (2), 273–279. doi:10.1007/s12034-014-0639-4

Sinha Ray, S., Dangayach, R., and Kwon, Y. N. (2021). Surface engineering for anti-wetting and antibacterial membrane for enhanced and fouling resistant membrane distillation performance. *Chemical Engineering Journal* 405, 126702. June 2020. doi:10.1016/j.cej.2020.126702

Tabhane, G. H., and Giripunje, S. M. (2020). Robust flower-like ZnO assembled β-PVDF/BT hybrid nanocomposite: Excellent energy harvester. *Polym. Test.* 88 (April), 106564. doi:10.1016/j.polymertesting.2020.106564

Tan, H. F., Tan, W. L., Hamzah, N., Ng, M. H. K., Ooi, B. S., and Leo, C. P. (2020). Membrane distillation crystallization using PVDF membrane incorporated with TiO2 nanoparticles and nanocellulose. *Water Sci. Technol. Water Supply* 20 (5), 1629–1642. doi:10.2166/ws.2020.068

Teoh, G. H., Ooi, B. S., Jawad, Z. A., and Low, S. C. (2021). Impacts of PVDF polymorphism and surface printing micro-roughness on superhydrophobic membrane to desalinate high saline water. *J. Environ. Chem. Eng.* 9 (4), 105418. doi:10.1016/j.jece.2021.105418

Tian, M., Zhu, J., Yuan, S., Zhang, Y., and Van der Bruggen, B. (2021). A co-casting route enables the formation of skinless, hydrophobic poly(vinylidene fluoride) membranes for DCMD. *J. Membr. Sci.* 630 (April), 119299. doi:10.1016/j.memsci.2021.119299

Tijing, L. D., Woo, Y. C., Choi, J. S., Lee, S., Kim, S. H., and Shon, H. K. (2015). Fouling and its control in membrane distillation-A review. *J. Membr. Sci.* 475, 215–244. doi:10.1016/j.memsci.2014.09.042

Tofighy, M. A., Mohammadi, T., and Sadeghi, M. H. (2021). High-flux PVDF/PVP nanocomposite ultrafiltration membrane incorporated with graphene oxide nanoribbones with improved antifouling properties. *J. Appl. Polym. Sci.* 138 (4), 49718–49815. doi:10.1002/app.49718

Wu, T., Zhou, B., Zhu, T., Shi, J., Xu, Z., Hu, C., et al. (2015). Facile and low-cost approach towards a PVDF ultrafiltration membrane with enhanced hydrophilicity and antifouling performance via graphene oxide/water-bath coagulation. *RSC Adv.* 5 (11), 7880–7889. doi:10.1039/c4ra13476a

Wu, X., Zhao, B., Wang, L., Zhang, Z., Li, J., He, X., et al. (2018). Superhydrophobic PVDF membrane induced by hydrophobic SiO2 nanoparticles and its use for CO2 absorption. *Sep. Purif. Technol.* 190, 108–116. doi:10.1016/j.seppur.2017.07.076

Xu, C., Chen, W., Gao, H., Xie, X., and Chen, Y. (2020). Cellulose nanocrystal/silver (CNC/Ag) thin-film nanocomposite nanofiltration membranes with multifunctional properties. *Environ. Sci. Nano* 7, 803–816. doi:10.1039/c9en01367a

Xuan, L., Tian, L. J., Tian, T., Wang, X. M., Yang, D. H., and Yu, H. Q. (2020). *In situ* synthesizing silver nanoparticels by bio-derived gallic acid to enhance antimicrobial performance of PVDF membrane. *Sep. Purif. Technol.* 251 (June), 117381. doi:10.1016/j.seppur.2020.117381

Zheng, L., Wu, Z., Wei, Y., Zhang, Y., Yuan, Y., and Wang, J. (2016). Preparation of PVDF-CTFE hydrophobic membranes for MD application: Effect of LiCl-based mixed additives. *J. Membr. Sci.* 506, 71–85. doi:10.1016/j.memsci.2016.01.044

Zhou, R., Rana, D., Matsuura, T., and Lan, C. Q. (2019). Effects of multi-walled carbon nanotubes (MWCNTs) and integrated MWCNTs/SiO 2 nano-additives on PVDF polymeric membranes for vacuum membrane distillation. *Sep. Purif. Technol.* 217 (February), 154–163. doi:10.1016/j.seppur.2019.02.013